Ballooning instability preventing the H-mode access in plasmas with negative triangularity shape on the DIII-D tokamak

IOP Publishing Ballooning instability preventing the H-mode access in plasmas…
Plasma Physics and Controlled Fusion **XX** (XXXX) XXXXXX https://doi.org/XXXX/XXXX

Ballooning instability preventing the H-mode access in plasmas with negative triangularity shape on the DIII-D tokamak

S. Saarelma[1,5], M.E. Austin[2], M. Knolker[1], A. Marinoni[1], C. Paz-Soldan[3], L. Schmitz[4], P.B. Snyder[1]

[1] General Atomics, San Diego, CA 92186-5608, USA
[2] The University of Texas at Austin, Austin, Texas 78712, USA
[3] Department of Applied Physics and Applied Mathematics, Columbia University, New York, NY 10027, USA
[4] Department of Physics and Astronomy, UCLA, Los Angeles, California 90095-1547, USA
[5] UK Atomic Energy Authority, Culham Science Centre, Abingdon, OX14 3DB, UK

E-mail: Samuli.saarelma@ukaea.uk

Received xxxxxx
Accepted for publication xxxxxx
Published xxxxxx

Abstract

Infinite toroidal mode number (n=∞) ballooning mode analysis of negative triangularity discharges on DIII-D shows that the access to 2nd stability becomes strongly restricted when the top triangularity decreases even modestly from -0.18 to -0.36. This is observed in experiment to coincide with the suppression of the L-H-transition. Further theoretical analysis with ballooning mode limited pedestals shows that the threshold for opening the 2nd stability access rises from a pedestal temperature of 0.3 keV to 1 keV when the top triangularity is decreased from -0.18 to -0.36 indicating that to access the 2nd stability with the more negative triangular shape would require unrealistically high pedestal temperature. The pedestal predicted by the EPED code agrees with the experimental H-mode profile for the negative triangularity case but in contrast to positive triangular shapes the prediction shows no increase in pedestal height with increasing core pressure when triangularity is negative. This work provides a first model to predict when negative triangularity plasmas can be expected to access the H-mode.

Keywords: negative triangularity, ballooning, LH-transition

1. Introduction

A tokamak fusion reactor has to achieve sufficiently long energy confinement together with high core plasma density and temperature. To achieve good energy confinement most researches in the last few decades have been concentrated on the so-called high confinement or H-mode [1]. In most plasma configurations, this operating mode offers a significant improvement in confinement over the so-called low confinement or L-mode. However, while in L-mode most of the energy flow escaping the plasma edge is driven by micro-turbulence leading to a constant energy flux into the scrape-off layer (the region just outside the confined plasma), in H-mode, part of the energy flow is driven by intermittent bursts in a form of Edge Localized Modes or ELMs that periodically collapse the steep pressure gradient region near the plasma edge called the pedestal [2]. As the ELMs release the energy

in short intense bursts, they can lead to unacceptable erosion on the divertor plates in reactor conditions. While there are certain H-mode operating conditions where the ELMs are avoided, such as the quiescent H-mode (QHM) [3] and the ELMs have been successfully suppressed by using external coils with resonant magnetic perturbations (RMP) [4], the robustness of such schemes in reactor conditions is yet to be demonstrated.

In H-mode, the turbulent transport makes the core temperature profiles more "stiff" ($\nabla T/T$ is close to threshold value). With stiff profiles the temperature profile is strongly influenced by the height of the pedestal temperature [5]. An alternative of trying to suppress the ELMs in H-mode plasmas is to operate the plasma in L-mode that is inherently ELM-free. Since the L-mode does not have the pedestal that is the source of the good confinement in H-mode, the only way to achieve comparable confinement of the plasma is to reduce the transport of particles and energy in the core region of the plasma. It has been shown on TCV [6,7] and DIII-D [8,9] that shaping a plasma cross section like a reversed D or having "negative triangularity" suppresses the turbulence in the core region of an L-mode plasma leading to confinement comparable to that of H-mode without the pedestal. This makes the negative triangularity regime a highly attractive option for a reactor [10, 11].

While there have been theoretical gyrofluid and gyrokinetic studies [6,7,12] showing the reduction of turbulent transport in the core region of negative triangularity plasmas, the question why the negative triangularity plasmas remain in L-mode has not been studied in detail. The recent experiments on DIII-D indicate extremely strong resilience of the negative triangularity plasmas to stay in L-mode well beyond the L-H-transition power threshold of similar plasmas with positive triangularity. In particular, it was found that a small increase in the top triangularity (δ_u) of the plasma (from -0.36 to -0.18) could trigger the L-H-transition at significantly lower auxiliary power than the more negative triangularity plasma (δ_u=-0.36) could be maintained in L-mode. The shapes of these two plasmas are shown in Fig 1.

In most L-H-transition studies the emphasis has been on the suppression of turbulence in the pedestal region. The prevailing paradigm for the L-H-transition is that the radially sheared E×B flow suppresses the turbulence [13] allowing formation of the steep pressure gradient or the pedestal near the plasma edge. The steep pressure gradient further increases the sheared rotation through diamagnetic drift effect leading to a positive feedback that leads to a sustained H-mode above a certain power threshold. In plasmas with positive triangularity this is possible because the ideal magnetohydrodynamic (MHD) stability limits restricting the steep pressure gradient are well above the gradients present in the L-mode plasmas. These limits are usually met only at much steeper gradients leading to ELMs as discussed above. In particular, pedestals with ELMs are usually found to be well above the pressure gradient limit of the n=∞ ballooning modes [14] that are found to theoretically limit the pressure gradient to a significantly lower value in circular large aspect ratio tokamaks. The high-pressure gradient region does not violate the ballooning stability limit because for shaped plasmas at low magnetic shear the plasma accesses the so-called second stability [15] where the ideal n=∞ ballooning mode stability limit for the pressure gradient completely disappears. In the pedestal region the magnetic shear is reduced by the bootstrap current driven by the steep pressure gradient.

However, if plasma bulges towards the low field side, the path length that the magnetic field line spends on the so-called bad curvature ($\nabla B^2 \cdot \nabla p > 0$) region of the plasma increases and this has a destabilizing effect on the ballooning modes [16]. In this paper we investigate the possibility that this destabilization of the ballooning modes is the reason why the negative triangularity plasma shape can substantially increase the power needed for the transition to the H-mode..

1.1 Earlier experiments with a bulge on the bad curvature side

When JT-60 installed its original divertor, it was localized on the low field side of the plasma [17,18]. The experiments with the outer divertor were able to produce short lived H-modes that improved the energy confinement time only by 10%. No good profile information of the density and temperature are available, but the analysis of the interferometer data indicated steepening of the density profile during the H-mode phase. The conclusion at the time was that the unfavorable shape did not prevent the H-mode access as had been predicted by the ballooning mode theory [18]. However, it must be noted that the JT-60 H-modes with the outer divertor never observed ELMs that were seen in experiments with the lower divertor and, which are a signature of the H-mode pedestal. It is therefore unclear if there indeed was a pedestal in the outer divertor plasmas or if the observed modest improvement of the energy confinement was due to some other reason.

In TCV, modest top negative triangularity ($\delta_u \approx -0.2$) discharges observed H-mode, but with significantly reduced pedestal top pressure compared to the positive triangularity shape. The result was consistent with the shallow pedestal being limited by the ideal MHD ballooning modes [19].

2. DIII-D experiments

The negative triangularity experiments at DIII-D were originally done with limited plasmas [7,8]. More recently,

experiments have been conducted with a lower single null divertor and negative triangularity shape in the top of the plasma [20]. We analyze in particular a pair of DIII-D single null discharges (#180533 and #180520) at I_p=0.9 MA, B_t=2.0 T with varying neutral beam heating, X-point at the bottom of the plasma and ∇B-drift in the favorable direction for the H-mode transition. The signals of top triangularity (δ_u), β_N, neutral beam heating power (PNBI), average density ($\langle n_e \rangle$) and D_α radiation from the divertor as well as the plasma shapes are shown in Fig. 1. Both discharges have negative top triangularity, but the important difference between them is that in one of them (#180520) the top triangularity is increased from -0.36 to -0.18 at 2200 ms (Fig. 2 showing the difference between the shapes). At this point with auxiliary heating power at 4 MW, the plasma immediately enters H-mode, which can be seen in increased density as well as the D_α recycling light showing distinct ELMs after the transition (Fig. 3). It must be noted that the small increase of triangularity at 2050ms leads to so called limit cycle oscillations (LCO) during which the edge density gradient increases, but only periodically and more modestly than in the robust ELMing H-mode that the discharge enters at 2200ms. The edge behaviour during LCOs in DIII-D is described more in detail in [21] and is not discussed further here.

In contrast, the heating power in the discharge with δ_u =-0.36 (#180533) increases up to 13MW but the discharge stays in L-mode. In this shot the divertor D_α signal shows limit cycle oscillation, but no clear drop in baseline or ELMs. In fact, in addition to NBI heating #180533 has a small amount (1.5MW) of electron cyclotron heating as well throughout the flat top phase of the discharge. The effect of that is negligible as a comparable discharge (#180519) without ECH behaves the same way. For comparison, the scaling for the L-H-transition [22] gives a value of 1.9 MW for the threshold power.

So, the L-H-transition threshold power increases at least from 4MW to 13MW when the shape changes only by the top triangularity decreasing from -0.18 to -0.36. It is possible that the difference is even larger as no H-mode was obtained with the δ_u=-0.36 shape. This indicates that the shape with highly negative triangular shape is very robust against the L-H-transition. While the divertor configuration may alter the L-H-threshold power significantly, the previous studies in DIII-D (elongation and X-point height [23, 24] and JET (positive values of upper triangularity) [25] regarding the shape dependence of the L-H-transition have shown only weak effects as long as the divertor configuration is not changed. The shaping effect on the required L-H-transition power observed here is significantly larger than what was found earlier. It appears to present itself as a sudden qualitative change rather than a gradual change in the L-mode turbulence. In the following we investigate if this could be due to an MHD stability limit to the edge pressure gradient, which is never observed in plasmas with zero or positive triangularity as the limit for these plasmas is well beyond the observed pressure gradient around the time of the L-H-transition.

3. n=∞ ballooning mode stability analysis

In the formalism for the local n=∞ ideal MHD ballooning mode stability [9] each flux surface can be treated individually, and its stability determined from a 1D equation. This allows a much more rapid solution of the stability than a full 2D stability analysis. For the stability analysis we use the BALOO code [26]. As a metric of equilibrium and stability limits stability limit, we use normalized pressure gradient α of the equilibrium flux surface defined as:

$$\alpha = \frac{\mu_0}{2\pi^2}\frac{\partial V}{\partial \psi}\left(\frac{V}{2\pi^2 R}\right)^{\frac{1}{2}}\frac{\partial p}{\partial \psi}, \qquad (1)$$

where μ_0 is the vacuum permeability, V is the volume enclosed by the flux surface, R is the major radius, ψ is the poloidal flux and p is the pressure. The stability limit is defined as how much α has to be increased beyond the equilibrium value before the flux surface becomes n=∞ ballooning mode unstable. BALOO artificially varies the local pressure gradient without changing the other equilibrium quantities to find the marginally unstable value of α. In case the flux surface is in the 2nd stability regime, there is no limit to α set by ballooning modes.

The n=∞ ballooning mode analysis of the effect of the shape in the experiment is done in two ways. First, we reconstruct the equilibria of the two experimental shapes, one in L-mode and one in H-mode using the measured profiles. From the ballooning stability diagrams of the two cases we can see if the stable access to H-mode type profiles changes with the shape change.

Second, we use the experimental plasma shapes but create the hypothetical profiles for a pedestal that is marginally stable against the 1st ballooning mode stability limit. Such a profile can be reconstructed with various density and temperature profiles, as replacing one with the other keeps the pressure gradient fixed. However, when the temperature is increased and density decreased, the collisionality decreases, which in turn increases the bootstrap current. The increasing bootstrap current lowers the magnetic shear and eventually opens the access to the 2nd stability. At that point, the ideal MHD n=∞ ballooning modes stop limiting the pedestal growth and the pedestal can increase (as long as the turbulence is suppressed) until the finite-n peeling-ballooning mode limit is reached, which represents the ultimate limit for the pedestal in H-mode. Substituting density gradient with temperature gradient is equivalent to increasing η_e ($= L_n/L_T \sim \nabla T/\nabla n$), where L_n and L_T are the gradient scale lengths of the density and temperature

profiles, respectively. Note that from pedestal turbulence simulations [27, 28] we know that increasing η_e will increase the turbulent transport. Consequently, if the required pedestal temperature for the opening of the 2nd stability access is too high, the η_e has to increase so much that the heat flux from turbulent transport will stop the growth of the temperature gradient before this is reached. On the other hand, once the 2nd stability access is opened, the density gradient can grow regardless of the temperature profile, which further suppresses the heat transport increasing the temperature gradient and bootstrap current and widening the 2nd stability access. The initial opening of the 2nd stability access is the key to unlock the virtuous cycle for the pedestal profiles. We now compare the required pedestal temperature for the two shapes for the opening of the second stability access.

3.1. Ballooning mode analysis using the experimental profiles

The profiles measured using the Thomson scattering diagnostic for electron density and temperature and charge exchange recombination spectroscopy for the ion temperature for the two discharges, #180533 and #180520 between 3400 and 3950 ms are shown in Fig. 4. The time period is chosen so that the H-mode case is well in the Type I ELM regime and the total β_N for the two cases is almost the same. For the H-mode data, only those Thomson scattering data are accepted that fall into the last 30% of the ELM cycle, while the L-mode data covers all the Thomson scattering data in the chosen time period. The raw data is fitted with a hyperbolic tangent function in the pedestal [29] and a smoothing spline in the core, which are then used in the equilibrium reconstruction. Note that while #180520 is in H-mode and has a clear pedestal structure in electron density and temperature but the ion temperatures are very similar in both cases.

Using these profiles to reconstruct the pressure profile, the self-consistent bootstrap current calculated using the formula in [30, 31] for the current and the shape taken from the EFIT reconstruction of the shots. We then vary the density and temperature profiles from L- to H-mode calculating a self-consistent equilibrium and calculate the distance to the stability boundary for both shapes. So, the profiles are described by the formula $f(\psi) = Hf_H(\psi) + (1-H)f_L(\psi)$, where f_H and f_L are the H and L-mode profiles and H varies between 0 and 1, with 0 indicating L-mode and 1 H-mode profiles. The normalized pressure gradient α and the stability boundaries with varying the temperature and density profiles from the experimental L- to H-mode profiles are shown in Fig. 5. In the plot the disappearance of the stability boundary indicates the access to 2nd stability. At the point where the profiles are composed of 40% H-mode and 60% L-mode profile, the more negative triangular shape (#180533, δ_u=-0.36) has a region that is unstable for the ballooning modes. The less negative triangular shape (#180520, δ_u=-0.18) stays stable and accesses the 2nd stability for the steepest pressure gradient region with 60% H-mode, 40% L-mode profiles. Even the more negative triangularity case would have 2nd stability access with full H-mode profiles, but before reaching that point it would have had a large section of the pedestal unstable to ballooning modes. As is shown in Fig 6 the q- and shear-profiles of the two plasma shapes with the profiles where the δ_u=-0.18 case access 2nd stability are very similar indicating that it is not differences in q that is responsible for the different stability behaviour.

If we plot only the stability of the flux surface ψ_N=0.978, the steepest part of the H-mode pressure gradient, as shown in Fig 7, we can see the variation of α and the stability boundaries along the transition from the L- to H-mode profiles. For the more negative triangular shape (#180533, δ_u =-0.36) the stability limit goes down as the pressure gradient increases and crosses the equilibrium value of α at about 25% of H-mode profile. On the other hand, with the less triangular shape (#180520, δ_u =-0.18) the stability limit first stays at constant value of α as equilibrium α increases and then accesses the 2nd stability as the profiles become more similar to H-mode profiles. The pedestal stays in the stable region throughout the transition. This indicates that the less negative triangular shape can access the H-mode profiles without violating the ballooning stability limit, while the more negative triangular shape cannot access the pressure profile of the H-mode pedestal without becoming ballooning mode unstable before that. It accesses 2nd stability in the steepest pressure gradient region only when a large part of the pedestal is unstable to ballooning modes.

Just to note here that if we repeat the above analysis with a mirrored positive triangularity shape, the pedestal is 2nd stable through the entire ranges plotted in Figs 5 and 7. This indicates that the access to 2nd stability comes to play in restricting L-H-transitions only in negative triangularity plasmas. In neutral or positive triangularity plasmas, the L-H-transition is controlled by other physical processes, most likely turbulence suppression through radially sheared E×B flow and the ballooning mode stability plays no role in it.

3.2. Marginally ballooning mode stable pedestal profiles

To get a more quantitative measure on how the pedestal profiles can access the 2nd stable region for ballooning modes when the plasma transitions from the L-mode to H-mode we generate artificial pedestal profiles that are stable against the 1st stability limit for the n=∞ ideal MHD ballooning modes. Since it is a limit for the pressure gradient, it does not uniquely define the profiles. So, we vary the ratio of temperature to

density to generate a range of profiles. As the temperature to density ratio increases, the collisionality decreases, which increases the bootstrap current, which in turn lowers the magnetic shear eventually opening up the access to 2nd stability for the ballooning modes. We can then compare the required temperature pedestal height for each shape to gain access to the 2nd stability. In this analysis, the temperature profile in the pedestal is assumed to have a hyperbolic tangent shape, $T(\psi_N) = C\left(1-\tanh\left(\frac{\psi_N-\psi_{mid}}{w}\right)\right)$, where ψ_N is the normalized poloidal flux, ψ_{mid} denotes the location of the middle of the pedestal and w is the width of the pedestal. In this analysis we assume $T_i=T_e$. The density profile is tailored so that each point in the pedestal is at the marginal stability for the ballooning modes. By varying the constant *C* we can vary the height of the temperature pedestal. As the temperature increases, we lower the density to keep the pedestal at marginal ballooning mode stability. At sufficiently high temperature, the shear reaches a point at some part of the pedestal where the 2nd stability access opens up and the ballooning limit for the pressure gradient disappears at that radial location. As it is impossible to continue the process that relies on profiles being ballooning limited beyond that point, we stop there and consider the profiles there as marginally 2nd stable density and temperature profiles. These profiles along with the H-mode profile of #180520 (δ_u =-0.18) are plotted in Fig. 8. The shape with less negative top triangularity (δ_u =-0.18) accesses the 2nd stability below the experimental H-mode temperature while the shape with more negative triangularity (δ_u =-0.36) requires $T_{e,ped}\approx$1.0keV to access the 2nd stability. This temperature pedestal is well above the experimental H-mode temperature pedestal. Furthermore, the density profile of the marginally 2nd stable δ_u =-0.36 is much lower than in the experiment, while in the δ_u =-0.18 case is very similar to the experimental profile. The scan reveals that in order for the δ_u =-0.36 to gain access to 2nd stability without violating the 1st stability limit along the way, the pedestal profiles have to be such that achieving them in L-mode plasma would be very difficult.

In addition to the top triangularity, the X-point position can affect the 2nd stability access. The above analysis was done using the experimental X-point location of R=1.66m. We now vary the radial location of the X-point and perform the same calculation of the marginal 2nd stability access for both values of top triangularity considered here. Fig. 9 shows how the 2nd stability access changes when the X-point is moved. Moving the X-point inwards has little effect on the 2nd stability access. The reason is that the ballooning modes locate themselves in the most unstable region of the plasma, which in this case is the top part of the plasma. Making the bottom part more stable makes little difference as the eigenfunction is very small in this region in any case. Moving the X-point moderately outwards (R=1.80m, corresponding δ_L=-0.2) has a slight destabilizing effect. At this point, the top part of the plasma still dominates the stability behavior. Moving the X-point slightly further out (R=1.85m, corresponding δ_L=-0.29) significantly increases the required pedestal temperature to open the 2nd stability access in both cases. This is the point where the bottom and top triangularities become similar, which means that the bottom negative triangularity starts contributing significantly to the destabilization of the ballooning modes. Moving the X-point even further out degrades the ballooning stability so much that no solution for the 2nd stability accessible profiles is found.

4. Finite-n Peeling-ballooning stability and pedestal prediction

The analysis of the n=∞ ballooning modes in the previous section showed that sufficiently negative triangularity closes the 2nd stability access and can therefore prevent the H-mode from developing into a robust ELMing state. It has been shown for various tokamaks that in H-mode the pedestal gradient is ultimately limited by ideal MHD peeling-ballooning modes leading to an ELM crash [32]. However, almost all such studies have been done for plasmas with positive triangularity. We test if the peeling-ballooning mode limit as the ultimate limit for H-mode pedestal applies also to the negative triangularity plasmas that reach H-mode and how much the stability limit is affected by the top triangularity. We analyze the finite-n ideal stability using the ELITE code [33]. For this purpose we generate a set of equilibria by varying the pedestal pressure gradient and current density around the experimental equilibrium while keeping the plasma shape, total current and stored energy fixed. The stability of each equilibrium is solved and for stability criteria separating the stable and unstable region we use $\gamma>\omega^*_{max}/4$, where γ is the growth rate of the fastest growing mode and ω^*_{max} is the maximum of the ion diamagnetic frequency in the pedestal.

The experimental points and the stability boundaries are shown in Fig. 10. First, we note that the small change in top triangularity has quite a significant effect on the stability boundary. The stability boundary of δ_u=-0.36 is about 30% lower in normalized pressure gradient than that of δ_u=-0.18. Second, the ELMing H-mode case (δ_u=-0.18) is within error margin from the stability boundary confirming that the peeling-ballooning mode boundary is limiting negative triangularity ELMing H-modes just as well as positive ones. Third, the more negative triangular L-mode case (δ_u=-0.36) remains deep in the stable region for peeling-ballooning modes, which is also consistent with the peeling-ballooning paradigm as it has no ELMs.

Next, we test the predictive EPED1 model [34] for the negative triangularity cases. EPED1 combines a simple scaling connecting the pedestal height ($\beta_{p,ped}$, the poloidal β of the pedestal top) and the width (Δ) by the condition $\Delta = 0.076\sqrt{\beta_{p,ped}}$) representing a kinetic ballooning mode limit for the pedestal with the finite-n ideal MHD peeling-ballooning mode stability limit to produce a prediction for the pedestal height and width. It is found to predict pedestal heights of several tokamaks within 20% statistical error [35]. However, except for a recent study for TCV [19] the EPED1 model predictions have not been tested for experimental negative triangularity plasmas.

The EPED1 analysis is done using the same global parameters as in the experiment studied in the previous section (B_t=2.0T, I_p=0.9MA). For simplicity we keep the shape of the plasma up-down symmetric in this study as we vary the triangularity from positive to negative values. The elongation is the same as in the experiment, 1.65. The shapes of the studied plasmas and the predicted pedestal temperatures for pedestal density of $n_{e,ped}=3\times10^{19}$ m^{-3} are shown in Fig. 11. The predicted pedestals are significantly lower for the negative triangularity shapes. Furthermore, they do not benefit from the stabilizing effect of the increasing Shafranov-shift seen in the positive triangularity cases. This agrees with the TCV results [19].

It must also be noted that the EPED1 predicted pressure using the same parameters and the same triangularity (the average of top and bottom triangularities) as in the experiment accurately predicts the pedestal pressure in the H-mode case described in sec. 3. The predicted and the experimental pressure profiles are shown in Fig. 12 with the δ=-0.1 corresponding the average triangularity of the experimental plasma shape. The prediction of the δ=-0.1 case agrees also with the EPED prediction done using the actual shape of the experimental plasma.

We can conclude from the EPED1 predictions that if the 2nd stability access in the pedestal can be obtained and the L-H-transition is triggered in negative triangularity plasmas, the resulting pedestal height will be low and does not increase with increasing plasma total energy. As the ELM energy fluence on the divertor targets is found to be roughly proportional to the pedestal pressure height [36, 37], this means that the transiently accessing H-mode in negative triangularity plasmas would not lead to large energy fluence from the ELMs but instead the ELMs would be relatively small. This adds a safety margin to operation in L-mode negative triangularity plasmas compared to other ELM suppression techniques that operate with large pedestals (eg. RMP ELM suppression). In these regimes the loss of ELM suppression generally results in a large ELM [38] and large energy fluence to the divertors, most likely leading to worse consequences.

5. Conclusions

We have shown that sufficiently negative top triangularity degrades the stability of the edge plasma for the n=∞ ballooning modes so that the access to the 2nd stability is closed and the pedestal pressure gradient is unable to exceed the ballooning stability limit. This prevents the virtuous cycle of pressure gradient driven diamagnetic rotation shear suppressing the turbulence and the reduced transport steepening pressure gradient. Without this bootstrapping mechanism the edge region does not enter H-mode but remains in L-mode even at high heating power.

We have also demonstrated that even a small change in the top plasma triangularity (δ_u =-0.18 to δ_u =-0.36) will lead to a significant increase in the required pedestal temperature to achieve the 2nd stability access and can explain the observation of plasma remaining in L-mode in the more negative triangularity shape at significantly higher heating power than where the less negative shape transitioned to H-mode.

In lower single null plasmas the closing of the 2nd stability access in plasmas with sufficiently negative top triangularity is relatively insensitive to the location of the X-point as long as the bottom triangularity stays positive or only modestly negative. Only if the X-point is moved sufficiently out in radius, the bottom part of the plasma also contributes to the closing of the 2nd stability access. This allows relative free divertor optimization based on other constrains, while using the top plasma shape to control the H-mode access.

The pedestal prediction using the EPED model shows that even if H-mode is accessed in negative triangularity plasmas it will have very modest pedestal height, which further reduces the danger of damaging the divertor components when operating the negative triangularity shaped plasmas in reactor conditions.

Acknowledgements

This work was supported in part by the US Department of Energy under DE-FC02-04ER54698, DE-FG02-95ER54309, DE-FG02-97ER54415 and DE-FG02-08ER54984.

References

[1] F Wagner, Plasma Phys. Controlled Fusion 49, B1 (2007)
[2] H Zohm, Plasma Phys. Control. Fusion, 38, 105 (1996)
[3] K H Burrell et al., Phys. Plasmas 12, 056121 (2005)
[4] T E Evans, R A Moyer, P R Thomas, T H Osborne, J A Boedo, E J Doyle, M E Fenstermacher, K H Finken, R J Groebner, M Groth, J H Harris, R J La Haye, C J Lasnier, S Masuzaki, N Ohyabu, D G Pretty, T L Rhodes, H Reimerdes, D L Rudakov, M J Schaffer, G Wang and L Zeng , Phys. Rev. Lett. 92 235003 (2004)
[5] C Holland, J E Kinsey, J C DeBoo, K H Burrell, T C Luce, S P Smith, C C Petty, A E White, T L Rhodes, L Schmitz, E J Doyle, J C Hillesheim, G R McKee, Z Yan, G Wang, L Zeng, B A Grierson, A Marinoni, P Mantica, P B Snyder, R E Waltz, G M Staebler and J Candy, Nucl. Fusion 53 (2013) 083027
[6] Y Camenen, A Pochelon, R Behn, A Bottino, A Bortolon, S Coda, A Karpushov, O Sauter, G Zhuang, and (TCV Team), Nucl. Fusion 47, 510 (2007)
[7] M Fontana, L Porte, S Coda, and O Sauter (TCV Team), Nucl. Fusion 58, 024002 (2018).
[8] M E Austin, A Marinoni, M L Walker, M W Brookman, J S deGrassie, A W Hyatt, G R McKee, C C Petty, T L Rhodes, S P Smith, C Sung, K E Thome, and A D Turnbull, Phys. Rev. Lett. 122 115001 (2019)
[9] A Marinoni , M E Austin , A W Hyatt, M L Walker, J Candy , C Chrystal , C J Lasnier, G R McKee, T Odstrčil, C C Petty , M Porkolab, J C Rost , O Sauter , S P Smith , G M Staebler, C Sung, K E Thome , A D Turnbull , L Zeng , and DIII-D Team, Phys. Plasmas 26, 042515 (2019)
[10] C Paz-Soldan to be submitted to Plasma Phys. Control. Fusion, arXiv:2012.03339v1
[11] M Kikuchi, T Takizuka, S Medvedev, T Ando, D Chen, J X Li, M Austin, O Sauter, L Villard, A Merle, M Fontana, Y Kishimoto and K Imadera, Nucl. Fusion 59 (2019) 056017
[12] A Marinoni, S Brunner, Y Camenen, S Coda, J P Graves,X Lapillonne, A Pochelon, O Sauter, L Villard, Plasma Phys. Control. Fusion 51 055016 (2009)
[13] H Biglari and P H Diamond, Phys. Fluids B: Plasma Physics 2, 1 (1990)
[14] J W Connor, R J Hastie and JB Taylor Proc. R. Soc. Lond. A3651–17 (1979)
[15] C M Bishop, P Kirby, J W Connor, R J Hastie and JB Taylor, Nucl. Fusion 24 1579 (1984)
[16] J M Greene, M S Chance, Nucl. Fusion, 21 453 (1981)
[17] H Nakamura, T Ando, H Yoshida, S Niikura, T Nishitani and K Nagashima, Nucl. Fusion 28 43 (1988)
[18] H Nakamura, T Ando, H Yoshida, S Niikura, T Nishitani, K Nagashima, Nucl. Fusion 30 235 (1990)
[19] A Merle, O Sauter, S Yu Medvedev, Plasma Phys. Control. Fusion 59 104001 (2017)
[20] A Marinoni et al. 28th IAEA Fusion Energy Conference, 10-15 May 2021, Nice, France, will be submitted to Nuclear Fusion.
[21] L Schmitz, L Zeng, T L Rhodes, J C Hillesheim, E J Doyle, R J Groebner, W A Peebles, K H Burrell, and G Wang, Phys. Rev. Lett. 108, 155002 (2012).
[22] Y Martin, T Takizuka and ITPA CDBM H-mode Threshold Database Working Group, J. Phys. Conf. Ser. 123 012033 (2008)
[23] T N Carlstrom, P Gohil, J G Watkins, K H Burrell, S Coda, E J Doyle, R J Groebner, J Kim, R A Moyer and C L Rettig, Plasma Phys. Control. Fusion 36 A147 (1994)
[24] P Gohil, T E Evans, M E Fenstermacher, J R Ferron, T H Osborne, J M Park, O Schmitz, J T Scoville, E A Unterberg, Nucl. Fusion 51 103020 (2011)
[25] Y Andrew N C Hawkes, M G O'Mullane, R Sartori, M de Baa, I Coffey, K Guenthe, I Jenkins, A Korotkov, P Lomas, Plasma Phys. Control. Fusion 46 A87 (2004)
[26] R L Miller, Y R Lin-Liu, A D Turnbull, V S Chan, L D Pearlstein, O Sauter, and L Villard, Phys. Plasmas 4 1062 (1997)
[27] D R Hatch M Kotschenreuther, S Mahajan, P Valanju and X Liu, Nucl. Fusion 57 036020 (2017)
[28] D R Hatch M Kotschenreuther, S M Mahajan, G Merlo, A R Field, C Giroud, J C Hillesheim, C F Maggi, C Perez von Thun, C M Roach, S Saarelma and JET Contributors, Nucl. Fusion 59 086056 (2019)
[29] R J Groebner, T H Osborne, Phys. Plasmas, 5, 1800 (1998)
[30] O Sauter C Angioni, Y R Lin-Liu, Phys. Plasmas 6 2834 (1999)
[31] O Sauter C Angioni, Y R Lin-Liu, Phys. Plasmas 9 5140 (2002)
[32] P B Snyder N Aiba, M Beurskens,, R J Groebner, L D Horton, A E Hubbard, J W Hughes, G T A Huysmans, Y Kamada, A Kirk, C Konz, A W Leonard, J Lönnroth, C F Maggi, R Maingi, T H Osborne, N Oyama, A Pankin, S Saarelma, G Saibene, J L Terry, H Urano, H R Wilson, Nucl. Fusion 49, 085035 (2009)
[33] H R Wilson, P B Snyder, G T A Huysmans and R L Miller, Phys. Plasmas 9 1277 (2002)
[34] P B Snyder, R J Groebner, A W Leonard, T H Osborne, and H R Wilson, Phys. Plasmas 16, 056118 (2009)
[35] P B Snyder, R J Groebner, J W Hughes, T H Osborne, M Beurskens, A W Leonard, H R Wilson, and X Q Xu, Nuclear Fusion, 51, 103016 (2011)
[36] T Eich, B Sieglin, A J Thornton, M Faitsch, A Kirk, A Herrmann, W Suttrop, Nucl. Mater. Energy 12, 84 (2017)
[37] M Knolker, A Bortolon, G P Canal, T E Evans, H Zohm, T Abrams, R J Buttery, E M Davis, R J Groebner, E Hollmann, M E Fenstermacher, C Lasnier, A W Leonard, R A Moyer, R Nazikian, T H Osborne, C Paz-Soldan, B Sieglin, Nucl. Fusion, 58, 096023 (2018)
[38] T E Evans, M E Fenstermacher, R A Moyer, T H Osborne, J G Watkins, P Gohil, I Joseph, M J Schaffer, L R Baylor, M Bécoulet, J A Boedo, K H Burrell, J S deGrassie, K H Finken, T

Jernigan, M W Jakubowski, C J Lasnier, M Lehnen, A W Leonard, J Lönnroth, E Nardon, V Parail, O Schmitz, B Unterberg and W P West, Nucl. Fusion 48 024002 (2008)

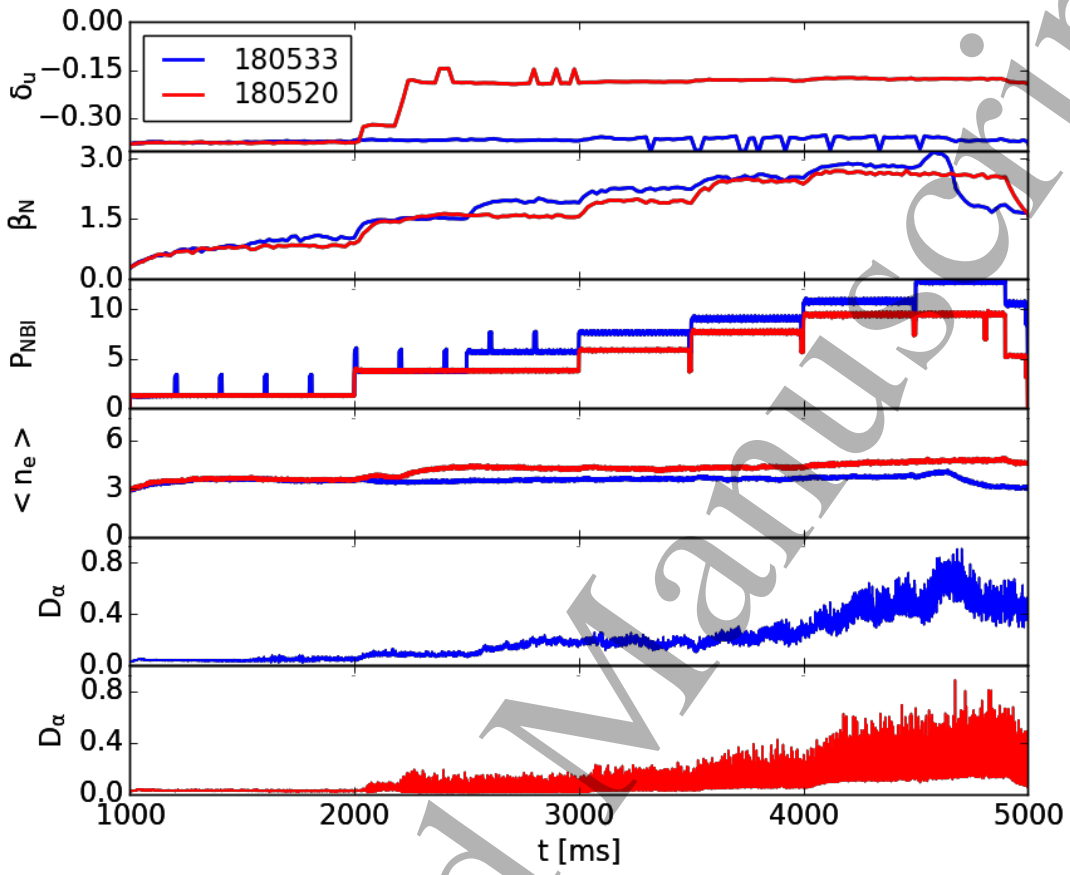

Figure 1. The time evolution of top triangularity, normalized β, neutral beam heating power (MW), average electron density (10^{19} m^{-3}) and divertor D_α radiation (a.u.) of the two DIII-D discharges. The discharge 180520 transitions to H-mode at about 2200ms.

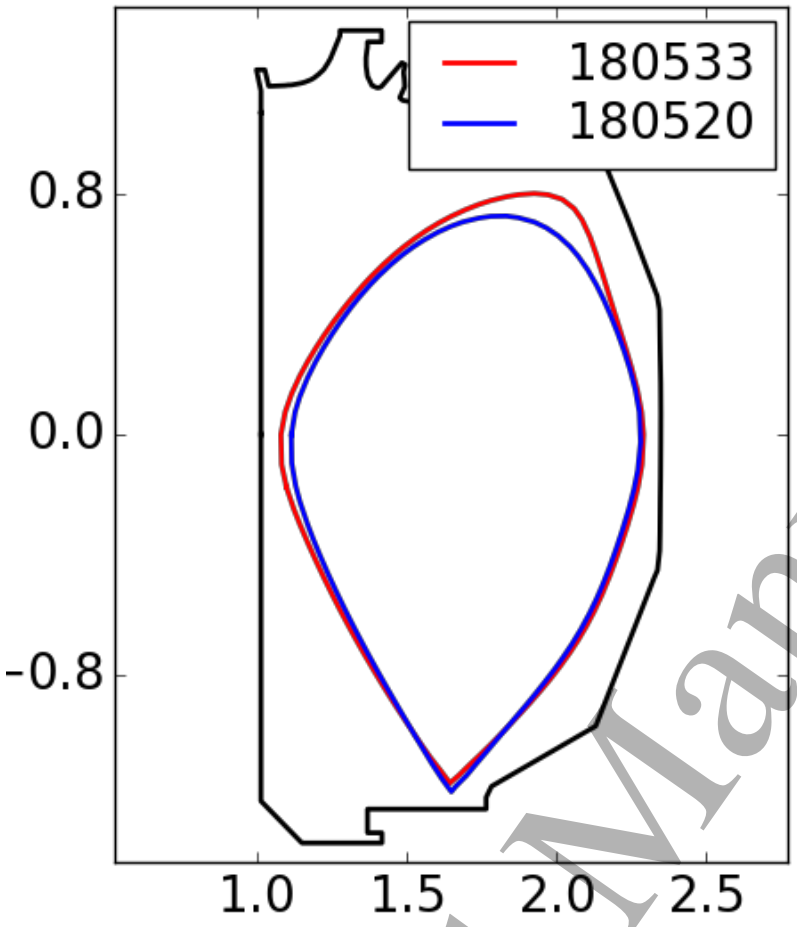

Figure 2. The plasma shapes of the DIII-D discharges 180533 (δ_u=-0.36, L-mode) and 180520 (δ_u=-0.18, H-mode).

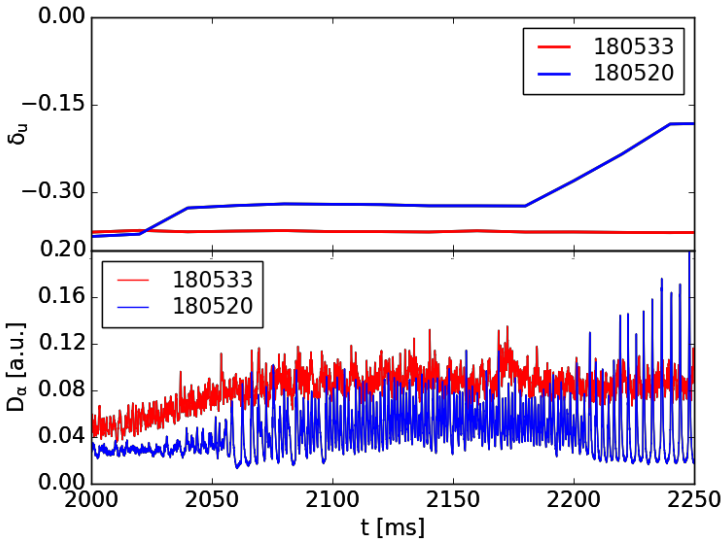

Figure 3. The top triangularity and the divertor D_a signal for the two discharges at the moment of the LH-transition in the 180520 discharge. The discharge with less negative triangularity (180520, δ_u=-0.18) shows distinctive ELMs after the transition while the discharge with more negative triangularity (180533, δ_u=-0.36) shows limit cycle oscillations.

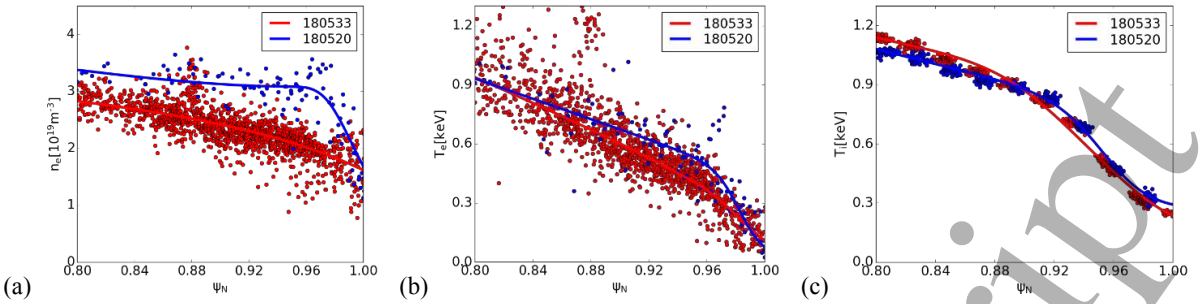

Figure 4. The pedestal electron density (a) and temperature (b) and ion temperature (c) profiles in the L-mode case (180533, δ_u=-0.36, red) and the H-mode case (180520, δ_u=-0.18, blue) as the function of normalized poloidal flux ψ_N. The solid lines show the fitted profiles used in the equilibrium reconstruction.

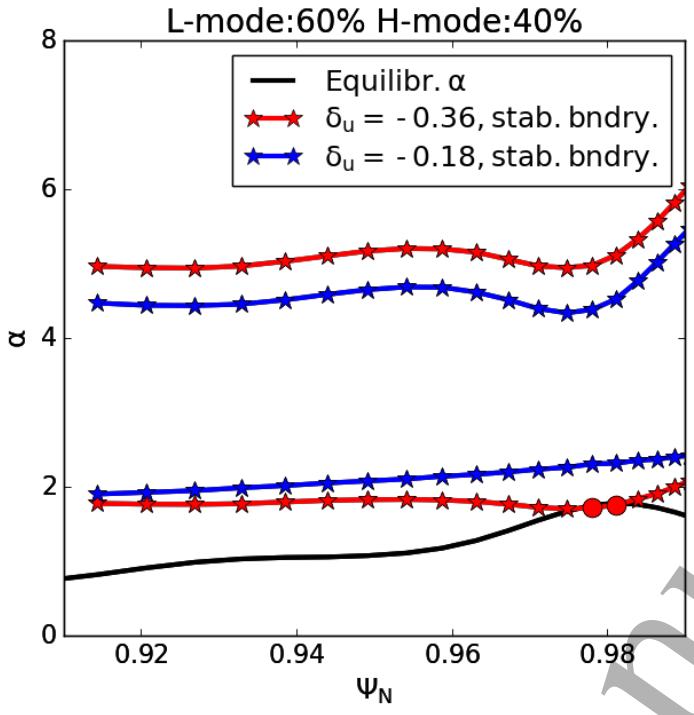

(a)

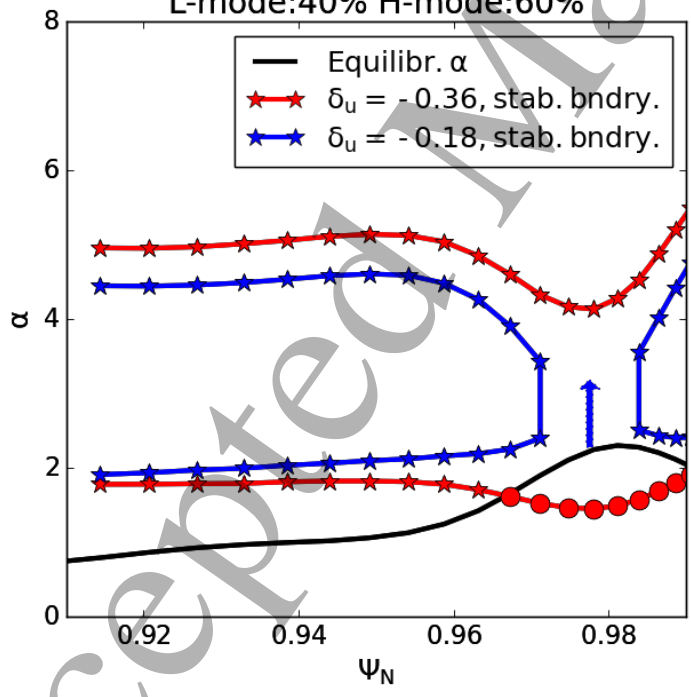

(b)

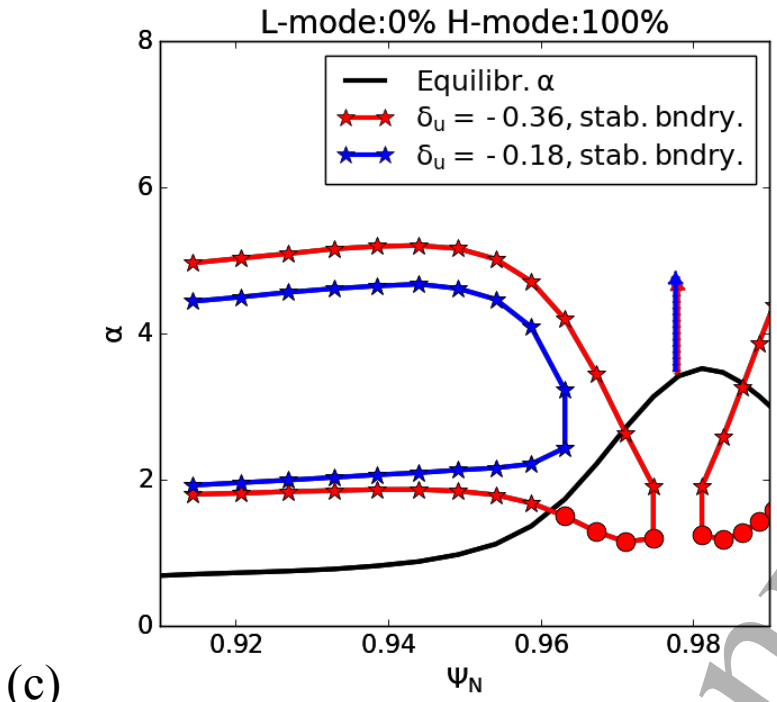

Figure 5. $n=\infty$ ballooning mode stability limits (lower is the 1st and the higher the 2nd stability limit and the region between them is unstable) and the equilibrium normalized pressure gradient α in the steep pressure gradient region for the two shapes #180533, δ_u=-0.18 (blue), #180520, δ_u=-0.36 (red) for three plasma profiles: with 60% L-mode, 40% H-mode profiles (a) with 40% L-mode, 60% H-mode profiles (b) and 100% H-mode profiles (c). The circles represent the equilibrium flux surfaces that are unstable and the arrow indicates that the equilibrium has access to the 2nd stability and the pressure gradient is not limited by n=∞ ballooning modes.

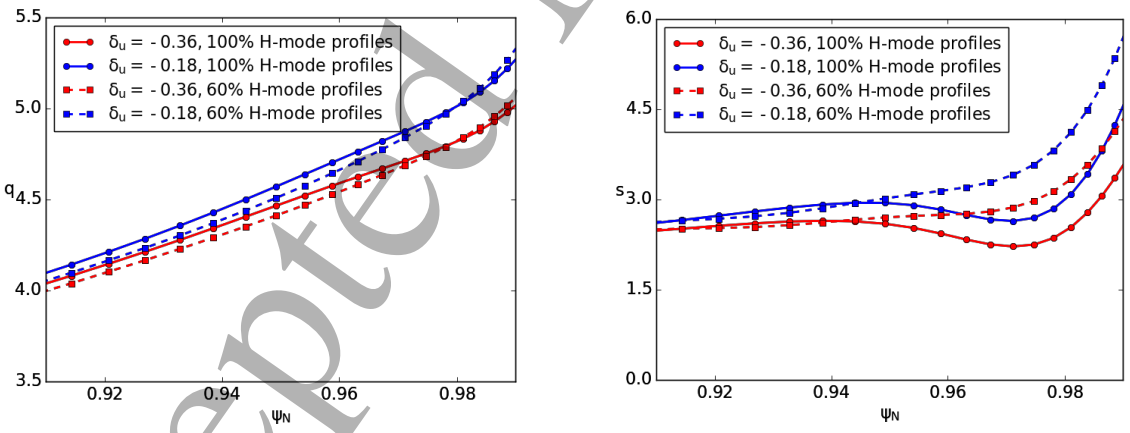

Figure 6. The q (left) and the shear (right) profiles of the two investigated plasma shapes #180533, δ_u=-0.18 (blue), #180520, δ_u=-0.36 (red) for two plasma profiles: with 40% L-mode, 60% H-mode (dashed) and 100 % H-mode (solid).

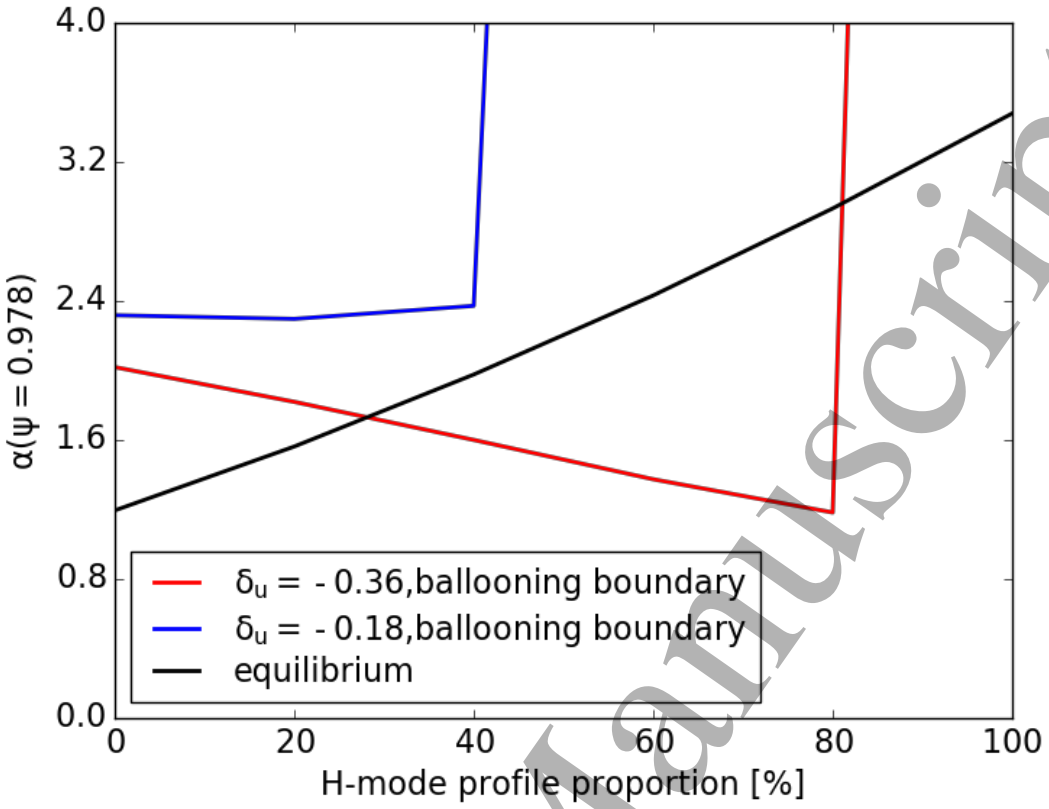

Figure 7 $n=\infty$ ballooning mode stability limits and the equilibrium normalized pressure gradient α at ψ=0.978 (the steepest part of the pressure gradient) for the two shapes #180533, δ_u=-0.18 (blue), #180520, δ_u=-0.36 (red) as a function of profiles transitioning from the L-mode profile to the H-mode profile. The crossing of the equilibrium line and the stability boundary indicates that the plasma becomes unstable. The stability boundary going vertical represents 2nd stability access.

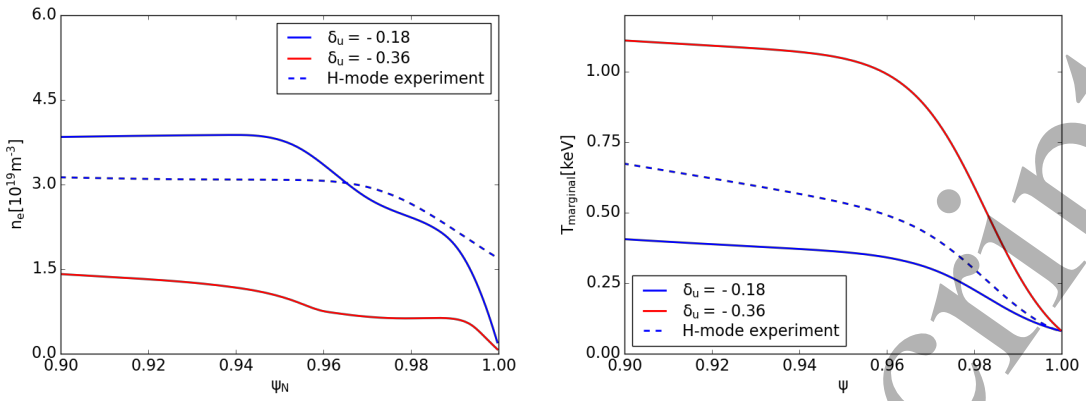

Figure 8. The density (left) and the temperature (right) profiles at the point where the pedestal marginally accesses the 2nd stability for n=∞ ballooning modes for the two experimental plasma shapes differing by the top triangularity. The dashed line shows the profiles of the H-mode case.

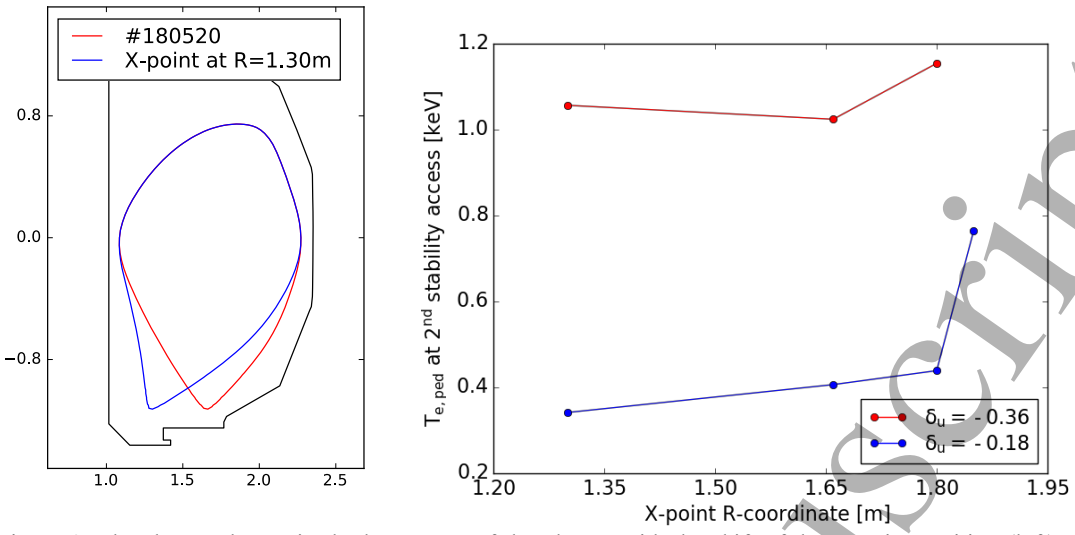

Figure 9. The shapes change in the lower part of the plasma with the shift of the X-point position (left) and the critical pedestal top temperature to open the 2nd stability access as a function of the X-point position for the two top triangularity values. The highest X-point value for the case 180533 is not plotted as no 2nd stability access was obtained for that shape.

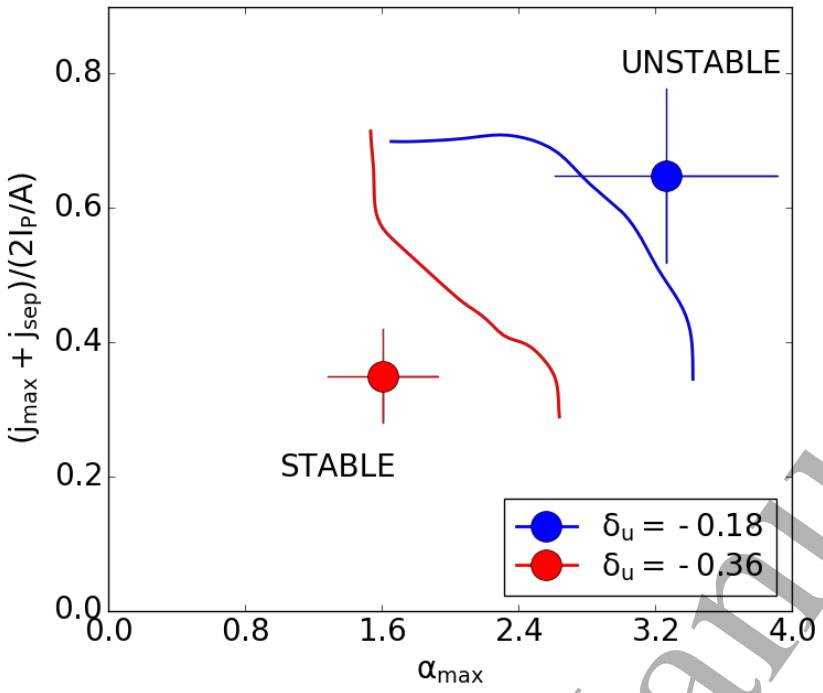

Figure 10. The experimental points (circles) and the finite-n peeling-ballooning stability boundaries (solid lines) of 180520 (δ_u=-0.18, blue) and 180533 (δ_u=-0.36, red) in normalized pressure gradient (x-axis) and normalized average current density in the pedestal (y-axis) space. The vertical and horizontal lines on the experimental point indicate the error margins of the measurement.

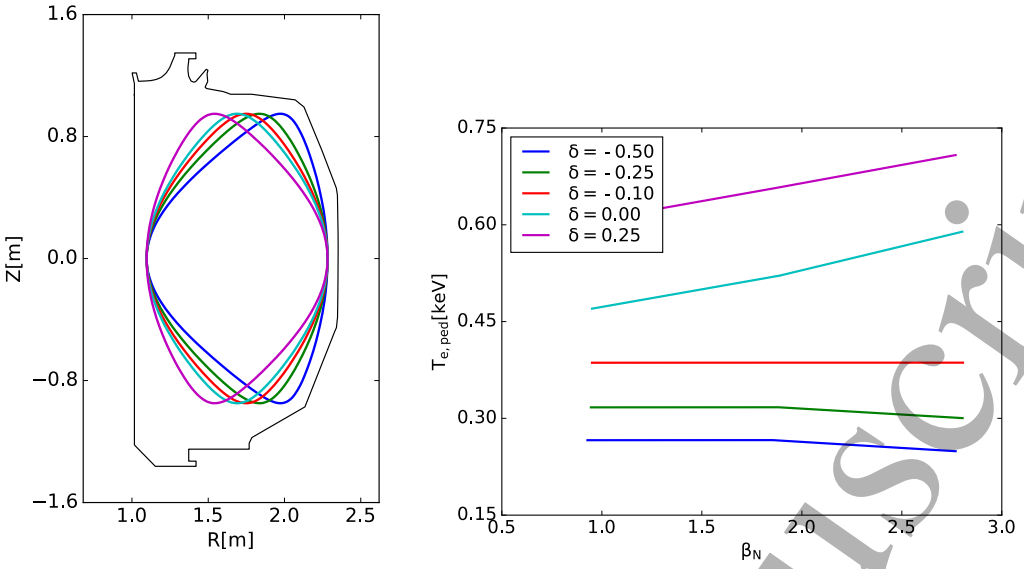

Figure 11. The plasma shapes used in the EPED1 prediction (left) and the predicted pedestal temperatures as a function of global β_N (right).

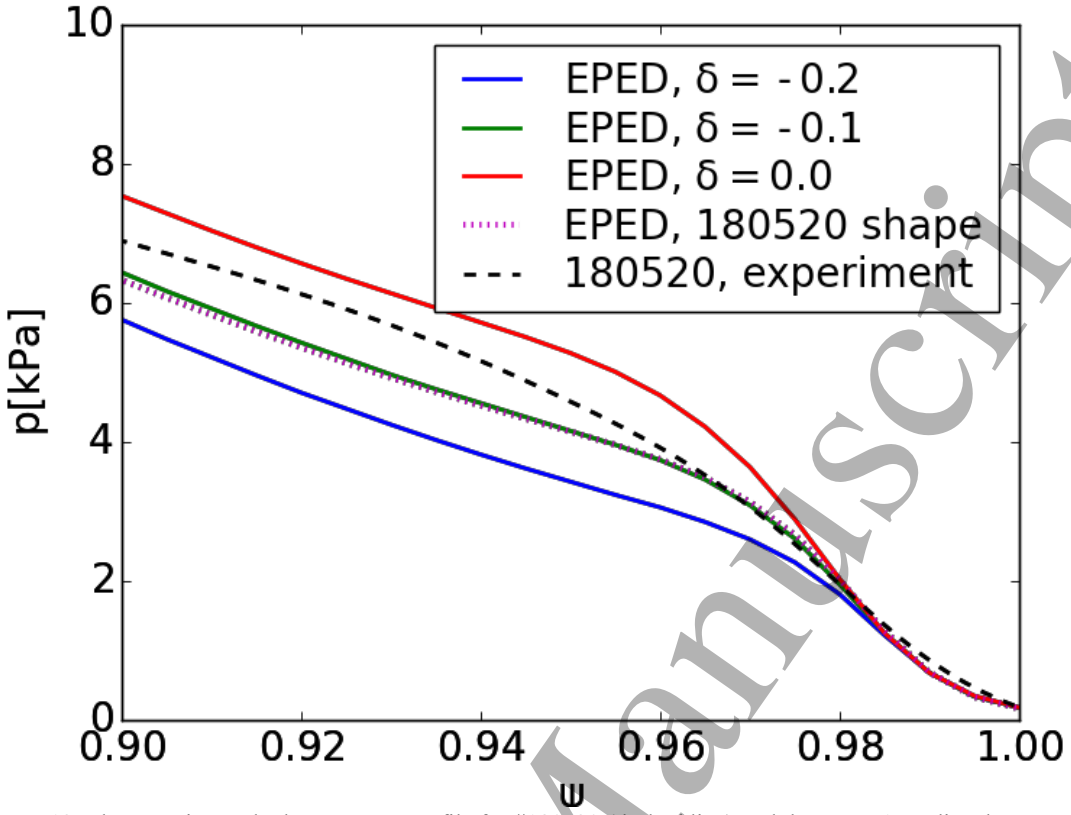

Figure 12. The experimental edge pressure profile for #180520 (dashed line) and the EPED1 predicted pressure profiles for the up-down symmetric case with three values of triangularity (solid line) and for the experimental shape (dotted line).